SAE INTERNATIONAL

ARTICLE INFO
Article ID: 08-08-01-0003

doi:10.4271/08-08-01-0003

Modeling and Optimal Design of All-Wheel-Drive Hybrid Light Trucks

Ziheng Pan,[1] Xiaowu Zhang,[2] Huei Peng,[1] and Nikhil Ravi[3]

[1]University of Michigan, USA
[2]Ford Motor Company, USA
[3]Robert Bosch LLC, USA

Abstract

Fuel economy and performance are both important in the design of hybrid pickup trucks. All-wheel drive is essential to ensure superior performance compared to two-wheel-drive designs. In this article, as a comprehensive extension work to the article published in ASME Dynamic Systems and Control Conference [1] on all-wheel-drive (AWD) hybrid truck, we investigate the modeling, design, and control problem of AWD hybrid vehicles and develop a methodology to identify optimal designs. This methodology 1) formulates an automated modeling process, 2) searches exhaustively through all possible AWD designs, and 3) employs a near-optimal energy management strategy, to obtain a family of designs with superior performance and fuel economy. A design case study for a hybrid Ford F-150 is conducted, to showcase this design process.

History

Received: 14 Sep 2018
Revised: 10 Jan 2019
Accepted: 16 May 2019
e-Available: 06 Jun 2019

Index Terms

All-wheel drive, Automated modeling, Hybrid electric vehicle design

Citation

Pan, Z., Zhang, X., Peng, H., and Ravi, N., "Modeling and Optimal Design of All-Wheel-Drive Hybrid Light Trucks," *SAE Int. J. Alt. Power.* 8(1):41–59, 2019, doi:10.4271/08-08-01-0003.

ISSN: 2167-4191
e-ISSN: 2167-4205

This article is based on an oral-only presentation at Dynamic Systems and Control Conference, Columbus, Ohio, October 28-30, 2015.

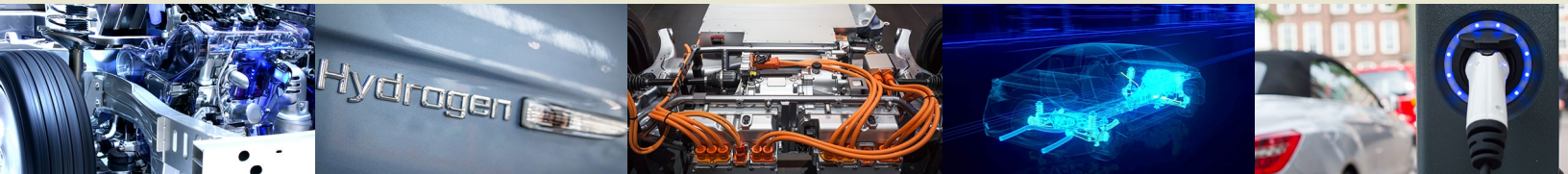

I. Introduction

Fuel efficiency continues to be a top priority for hybrid vehicles, because of the concerns on CO_2 emissions and climate change. As shown in Table 1 [2], the estimated average fleet-wide fuel economy in the USA will be 55.3-56.2 mpg for passenger cars and 39.3-40.3 mpg for light trucks in 2025. Different technologies were investigated trying to meet this stringent standard [3, 4, 5, 6]. Among them, hybrid powertrain is a promising alternative to achieve these requirements, and its successful implementation on passenger cars, such as Toyota Prius, Ford Fusion, and Chevy Volt, have shown significant fuel economy improvement (see in Table 2 [7]). In contrast, few strong hybrid light-truck-class vehicles have been made available. Few exceptions include UPS hybrid delivery trucks [8] or the Toyota RAV4 Hybrid SUV [9].

To design hybrid trucks is more challenging than hybrid passenger cars. Tighter performance requirements, including launching, towing, and uphill grade, are expected. For example, SAE established minimum performance requirement for tow vehicles like light trucks known as the SAE Standard J2807 [10]. Much of the existing literature and patents for hybrid trucks mainly focus on configuration design and control to reduce fuel consumption [11, 12, 13]. Recently, a few publications have included launching performance in addition to fuel economy as the design requirement for hybrid vehicles [14, 15].

To accomplish the tight performance together with the fuel economy goal, pickup truck designs with all-wheel-drive (AWD) are preferred. Designs with AWD have better gradeability and towing capacity than comparable rear-wheel-drive (RWD) designs especially on an uphill slope, as shown in Figure 1. Therefore, AWD is a highly desirable design feature for hybrid pickup trucks or similar light-duty applications. An example AWD hybrid design available on the market for similar applications is the Acura RLX Sport Hybrid [16] shown in Figure 2. This parallel hybrid design has three electric motors, with two motors on the rear axle coupled with the front axle through the road. Toyota RAV4 Hybrid SUV [9] and the Lexus RX Hybrid [17] are power-split hybrid designs among the very few AWD hybrid vehicles available on the market today. In both cases, to enable AWD feature, a third motor is added to the rear wheels for these two models.

Different from the designs of Honda and Toyota which achieve AWD feature by adding motor(s) to rear wheels, this article focuses on AWD power-split hybrid powertrains that use two electric motors and couple all components mechanically directly through planetary gear (PG) sets, which have not been systematically studied before. Power-split-type hybrid powertrain is highlighted because it has secured over 80% of the hybrid passenger car market share in the USA [18], among all three types of hybrid powertrains (series, parallel, and power-split types). Two PGs are required for an AWD power-split hybrid powertrain to connect all elements (i.e., an engine, two motors, front output shaft, and rear output shaft).

TABLE 1 Required fleet-wide fuel economy (mpg) under future CAFE standards. Reprinted with permission from Ref. [2].

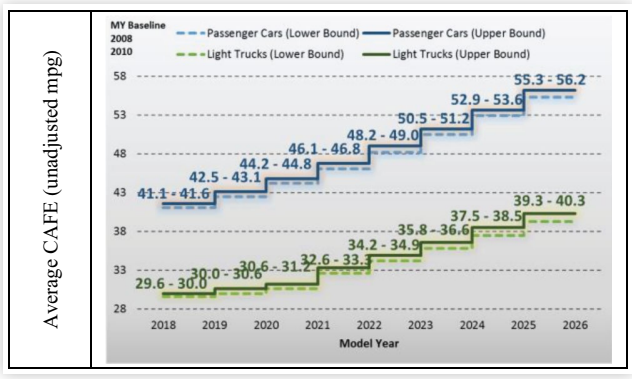

TABLE 2 Fuel economy (mpg) performance comparison examples between conventional passenger cars and power-split hybrid passenger cars. Reprinted with permission from Ref. [6].

Vehicle model	Powertrain type	Powertrain specs	Combined fuel economy (mpg)
2018 Toyota Camry	Conventional - automatic transmission	2.5 L, 4 cyl, AT (S8)	32
2018 Ford Fusion FWD		2.5 L, 4 cyl, AT 6-spd	25
2018 Chevrolet Volt	Power-split hybrid	1.5 L, 4 cyl, CVT	E: 106 MPGe/42MPG
2018 Ford Fusion Hybrid		2.0 L, 4 cyl, CVT	42
2018 Toyota Prius		1.8 L, 4 cyl, CVT	52
2018 Toyota Camry Hybrid		2.5 L, 4 cyl, CVT	52

FIGURE 1 Launching and towing performance comparisons of AWD and RWD vehicles designs on a slope.

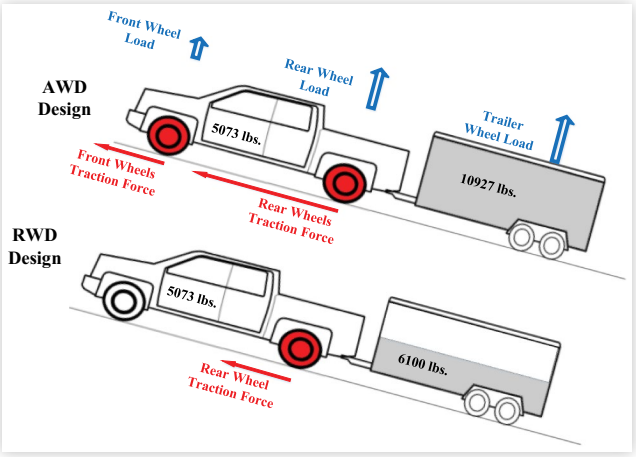

FIGURE 2 Design schematic of the Acura RLX Sport Hybrid [16].

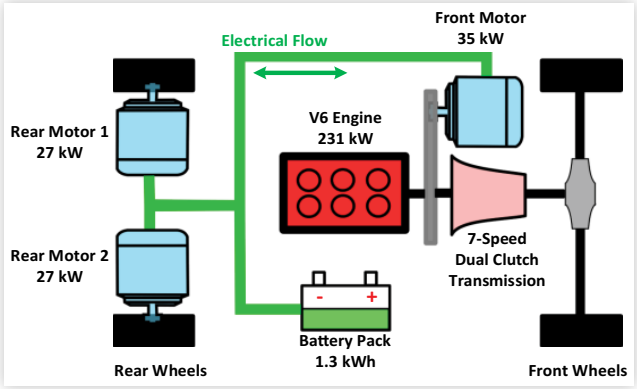

This article presents systematic and exhaustive studies on designs of AWD power-split hybrid powertrain for pickup trucks to achieve both good fuel economy and launching performance. In addition to the AWD attribute, other attributes might be specified, such as all-wheel-regenerative braking (AWRB) and driving backward using the engine power. Multi-mode attribute is also enabled by adding clutches into the powertrain, which is important to improve fuel economy performance [15, 19, 20].

Prior studies indicated that there exist a large number of possible designs using a double PG set for hybrid vehicles [13, 19, 20, 21]. In addition, when component sizing is considered, the overall design space to be searched becomes extremely large, i.e., over ten million possibilities in the case study to be presented in this article. In order to search the design space thoroughly, a four-step methodology is proposed by applying the following techniques:

> A generic representation that enables automated modeling for all possible configurations and operating modes; A systematic screening method to exhaustively search and examine for feasible designs; An optimization scheme to optimize for the fastest launching performance; A near-optimal energy management algorithm that evaluates fuel economy of feasible designs at a computational efficient manner [20].

With the above techniques, systematic screening and analysis of AWD power-split hybrid designs become possible, and a family of optimal designs can be identified.

In the design procedure, a near-optimal energy management is important to evaluate the fuel economy of design candidates efficiently. Popular control strategies studied in the past include rule-based strategies [22], Equivalent Consumption Minimization Strategy (ECMS) [23, 24], Dynamic Programming (DP) [25, 26], and Power-weighted Efficiency Analysis for Rapid Sizing (PEARS) [20]. They all have advantages and disadvantages. Many of the existing optimization methods, such as ECMS, PMP, and fuzzy logic, are not designed to solve this non-convex mixed integer optimization problem. DP can be used to solve the control problem for this multi-mode hybrid powertrain, but it suffers from its curse of dimensionality and it takes too long to handle a large amount of cases. The PEARS method is selected for this article because of its near-optimality and its ability to handle a large number of design candidates at fast computational speed.

The major contribution of this article is the development of an exhaustive design process for AWD multi-mode power-split hybrid vehicles that achieve optimal fuel economy while satisfying performance constraints, which includes a generic representation of the powertrain, a systematic screening method, and an optimization scheme for performance evaluation, and adaptation of a near-optimal energy management algorithm for fuel economy evaluation. This article extends previous work [1], enables to screen all powertrain components' size (engine, electric motors, transmission ratio, etc.), and provides comprehensive analysis for this AWD power-split powertrain. The remainder of this article is organized as follows: Section II introduces the concept of the four-step systematic design process; Section III describes the dynamic model of AWD power-split hybrid powertrains; Section IV presents the automated modeling technique to model all designs sharing similar dynamic structure in Section III; Section V shows how to screen for desired designs satisfying performance requirement; Section VI introduces problem formulation and the PEARS method; Section VII presents the feasible designs and simulation results; Section VIII analyzes the performance of the identified AWD hybrid design; and finally Section IX summarizes this article.

II. Four-Step Systematic Design Process

The design problem for optimal configurations, sizing, and control can involve a very large number of design candidates. Brute force searching would require tens of thousands of fast computer cores, and this is neither necessary nor efficient. Given this large number of design pool, we proposed a four-step systematic design process which starts by screening out infeasible or incapable designs. The number of design candidates requiring heavy computations is then significantly reduced, and evaluation for their performance become possible.

This four-step design process is summarized in Figure 3.

Step 1 - Automated modeling: A proposed procedure to model all modes of all possible AWD designs, based on the powertrain dynamics incorporated with clutch connection modeling [27]. We limit the design space to designs that use three clutches.

Step 2- Performance screening: A step to screen modeled designs for desired attributes and criteria. Performance attributes are functionalities required by the designer and can include but not limited to

FIGURE 3 Four-step systematic design process.

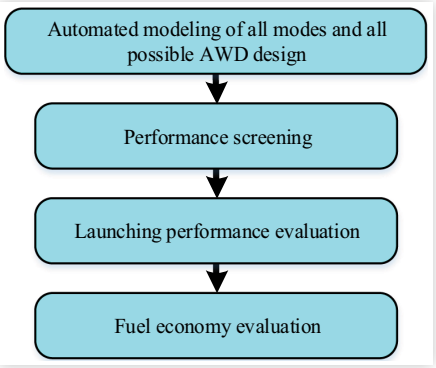

AWD, all-wheel regenerative braking, driving backward using the engine power, etc. Performance criteria can include acceleration time, towing capability on a slope, gradeability, etc. Criteria can be based on standards like the SAE Standard J2807 for light trucks or demanded by designers. Designs that survive from this step are called *feasible* designs. This screening step is critical to weed out inferior designs so that only feasible designs are passed to future steps.

Step 3- Launching performance evaluation: An evaluation procedure to obtain the best launching performance for each design. The best launching performance is defined in terms of 0-60 mph acceleration time. It is obtained by solving a linear optimization problem.

Step 4- Fuel consumption evaluation: An evaluation procedure to obtain the best fuel economy for each design given standard drive cycles. This evaluation is formulated as an optimization and solved by DP incorporating the PEARS method [20].

Terms frequently used in this article are defined in Table 3.

TABLE 3 Terms frequently used for the systematic design process.

Terms	Definition
Node	The available collocation points of the PG sets (i.e., sun, carrier, and ring gears)
Configuration	A given topology how components (i.e., engine, motors, output shafts) connected with the nodes
Design	A configuration plus a selected set of clutches
Design candidate	A design with given component sizing (e.g., gear ratios for the PG set and final drive ratio)
Mode	The clutch states (i.e., open and close)

III. Modeling of AWD Power-Split Hybrid Powertrain

In this article, AWD power-split hybrid vehicle powertrain candidates consist of an internal combustion engine, two electric motors, a battery pack, two PG sets, two output shafts, and three clutches. Figure 4 illustrates an example design of AWD power-split architecture patented by Toyota [28]. The double PG set acts as a continuous variable transmission (CVT). The engine speed can be controlled by the MG1 motor for optimal engine operation. The engine drives both front and rear wheels while the MG2 motor adjusts the torque difference between front and rear wheels. The following part of this section develops the systematic modeling of this class of AWD power-split hybrid powertrains.

All power-split hybrid powertrain including the example in Figure 4 can be modeled through matrix representation. This technique is used throughout this research for modeling and simulating the powertrain dynamics, and also for design screening. In Equation 1, this technique is used to present the dynamics of the Toyota patented example in Figure 4, where $T_{(\cdot)}$ denotes components' torque, $\dot{\omega}_{(\cdot)}$ is the angular acceleration, $I_{(\cdot)}$ is the corresponding inertia, $F_{(\cdot)}$ denotes internal gear force of the corresponding PG set, and $R_{(\cdot)}$ and $S_{(\cdot)}$ are the radii of the ring gear and the sun gear.

$$\begin{bmatrix} I_e+I_{c1} & 0 & 0 & 0 & 0 & 0 & R_1+S_1 & 0 & 0 \\ 0 & I_F+I_{c2} & 0 & 0 & 0 & 0 & 0 & R_2+S_2 & 0 \\ 0 & 0 & I_R+I_{mg2}+I_{s2} & 0 & 0 & 0 & 0 & -S_2 & 0 \\ 0 & 0 & 0 & I_{mg1}+I_{s1} & 0 & 0 & -S_1 & 0 & 0 \\ 0 & 0 & 0 & 0 & I_{r1} & 0 & -R_1 & 0 & 1 \\ 0 & 0 & 0 & 0 & 0 & I_{r2} & 0 & -R_2 & -1 \\ R_1+S_1 & 0 & 0 & -S_1 & -R_1 & 0 & 0 & 0 & 0 \\ 0 & R_2+S_2 & -S_2 & 0 & 0 & -R_2 & 0 & 0 & 0 \\ 0 & 0 & 0 & 0 & 1 & -1 & 0 & 0 & 0 \end{bmatrix} \cdot \begin{bmatrix} \dot{\omega}_e \\ \dot{\omega}_F \\ \dot{\omega}_R \\ \dot{\omega}_{mg1} \\ \dot{\omega}_{r1} \\ \dot{\omega}_{r2} \\ F_1 \\ F_2 \\ T_{cl1} \end{bmatrix} = \begin{bmatrix} T_e \\ -T_F \\ -T_R+T_{mg2} \\ T_{mg1} \\ 0 \\ 0 \\ 0 \\ 0 \\ 0 \end{bmatrix} \quad \text{Eq. (1)}$$

The matrix representation for complete dynamics in Equation 1 contains both the kinetics and kinematics of the system. Its uniqueness of each design enables automated modeling possible; its content information of components' connection allows screening and mode analysis; the complete dynamics can be used to evaluate the response of the powertrain.

FIGURE 4 An example AWD power-split hybrid vehicle design from the Toyota patent. Reprinted with permission from Ref. [27].

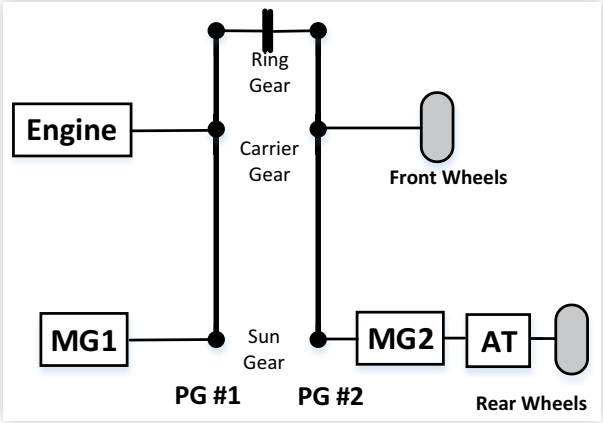

More details of deriving and utilizing this representation to develop the mathematical models of the components and the integrated system can be found in this and the next chapter.

A. Vehicle Model

A quasi-static model is used to simulate the dynamics of the vehicle. Figure 5 shows the free-body diagram for the longitudinal vehicle motion on a flat road, where the vehicle has a body mass m_b (without wheels) and the wheel mass m_w for both front and rear axles. The wheel inertia is denoted as I_w. The gravitational constant is g, and the aerodynamic force is D_A.

FIGURE 5 Free-body diagram for the longitudinal vehicle motion on a flat road.

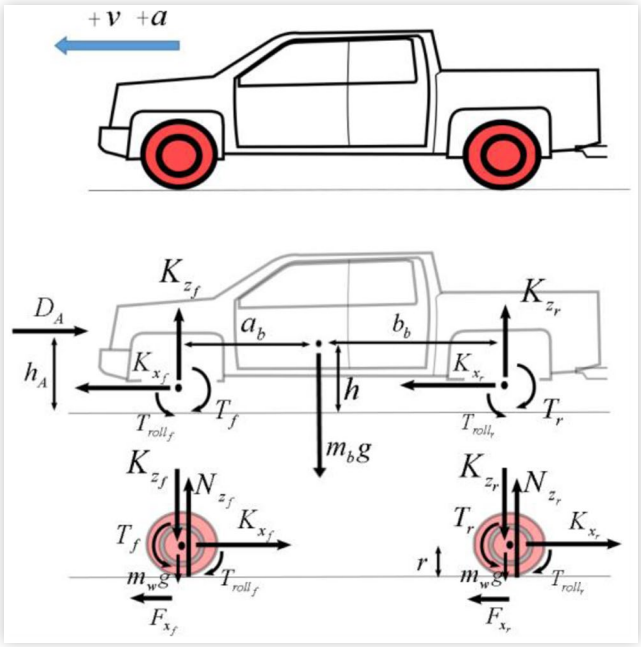

T is the axle output torque, K_z is the vertical force between the wheels and body, K_x is the longitudinal force between the wheels and body, N_z is the tire reaction force in the vertical direction, and F_x is the tire reaction force in the longitudinal direction. The subscripts f and r refer to the front and rear axles, respectively.

Longitudinal dynamics and rotational motion dynamics of the vehicle body, front wheels, and rear wheels are given in Equations 2 through 10.

$$K_{x_f} + K_{x_r} - D_A = m_b a \quad \text{Eq. (2)}$$

$$K_{z_f} + K_{z_r} = m_b g \quad \text{Eq. (3)}$$

$$\begin{aligned} &-K_{z_f} a_b + K_{z_r} b_b - D_A (h_A - h) \\ &-\left(K_{x_f} + K_{x_r}\right)\cdot(h - r) \\ &+ T_f - T_{roll_f} + T_r - T_{roll_r} = 0 \end{aligned} \quad \text{Eq. (4)}$$

$$T_f - F_{x_f} r - T_{roll_f} = I_w \dot{\omega}_f \quad \text{Eq. (5)}$$

$$F_{x_f} - K_{x_f} = m_w a \quad \text{Eq. (6)}$$

$$N_{z_f} - K_{z_f} - m_w g = 0 \quad \text{Eq. (7)}$$

$$T_r - F_{x_r} r - T_{roll_r} = I_w \dot{\omega}_r \quad \text{Eq. (8)}$$

$$F_{x_r} - K_{x_r} = m_w a \quad \text{Eq. (9)}$$

$$N_{z_r} - K_{z_r} - m_w g = 0 \quad \text{Eq. (10)}$$

By defining the total mass M, the total rolling resistance T_{roll}, a rear-to-front torque ratio α between T_f and T_r in Equations 11 through 13, these two axle output torques can be expressed in Equations 14 and 15.

$$M = m_b + 2m_w \quad \text{Eq. (11)}$$

$$T_{roll} = T_{roll_f} + T_{roll_r} \quad \text{Eq. (12)}$$

$$T_f = T_r \alpha \quad \text{Eq. (13)}$$

$$T_f = \frac{\alpha}{\alpha+1}\left[Mar + I_w\dot{\omega}_f + I_w\dot{\omega}_r + T_{roll} + D_A\right] \quad \text{Eq. (14)}$$

$$T_r = \frac{1}{\alpha+1}\left[Mar + I_w\dot{\omega}_f + I_w\dot{\omega}_r + T_{roll} + D_A\right] \quad \text{Eq. (15)}$$

The aerodynamic force in Equations 14 and 15 can be calculated by

$$D_A = \frac{1}{2}\rho C_d A_{aero} v^2 \quad \text{Eq. (16)}$$

where ρ is the air density, C_d is the drag coefficient, and A_{aero} is the maximum vehicle cross-sectional area. In this article, the tire slip is not considered. Hence, all wheels have the same angular speed shown in Equation 17.

$$\omega_f = \omega_r = \frac{v}{r} \quad \text{Eq. (17)}$$

B. Engine and Electric Motor Model

The fuel rate consumed $\dot{m}_f$ is obtained from a look-up table calculated from a Brake-Specific Fuel Consumption (BSFC) map of the 3.6L boosted engine, which is shown in Figure 6. Constraints of engine speed ω_e and torque T_e are indicated in the BSFC map and considered throughout the design process.

Similarly, efficiency of the two electric machines is obtained from the look-up table shown in Figure 7. Given the electric motor torques, T_{MG1}, T_{MG2}, and motor speeds, ω_{MG1}, ω_{MG2}, the power of the two electric machines is expressed in

FIGURE 6 Engine BSFC map.

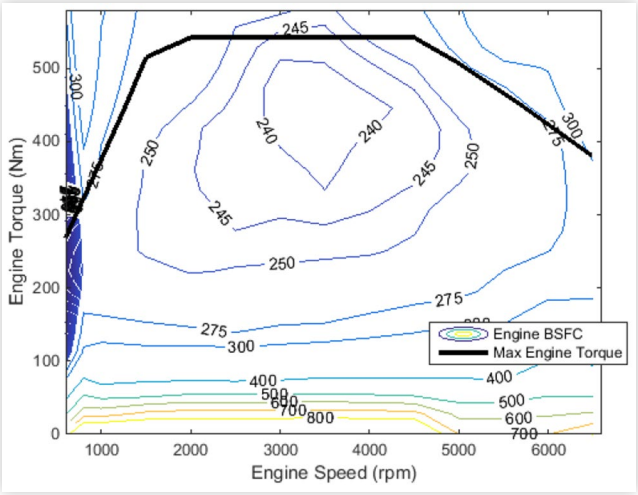

FIGURE 7 Efficiency map of the electric motor.

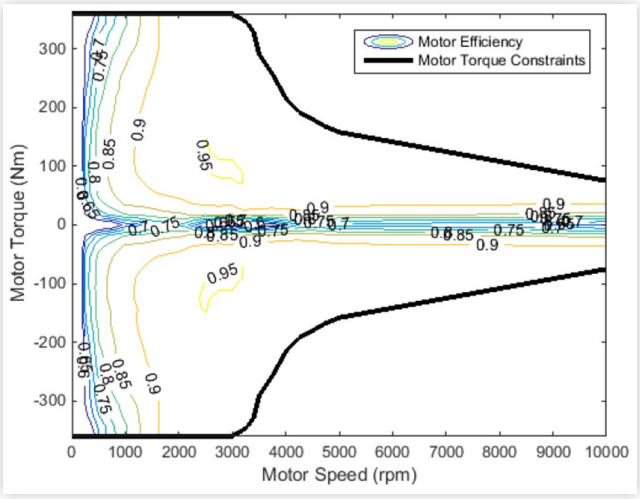

Equation 18, where η_{MG1}^{k1} and η_{MG2}^{k2} are the efficiency of the two motors, respectively. *k1* and *k2* will be -1 if the electric machine is motoring and 1 if it is generating.

$$P_{elect} = T_{MG1}\omega_{MG1}\eta_{MG1}^{k1} + T_{MG2}\omega_{MG2}\eta_{MG2}^{k2} \quad \text{Eq. (18)}$$

C. Battery Model

The battery is modeled as a simple open-circuit voltage with a constant internal resistance. The battery state of charge (SOC) is described in Equation 19.

$$\dot{SOC} = -\frac{V_{oc} - \sqrt{V_{oc}^2 - 4R_{bat}P_{elect}}}{2 \cdot R_{bat}} \quad \text{Eq. (19)}$$

D. PG Model

A typical PG set is shown in Figure 8 together with its equivalent lever diagram. The three nodes in the lever diagram represent the ring gear, carrier, and sun gear of this PG, respectively.

FIGURE 8 PG set and its lever diagram.

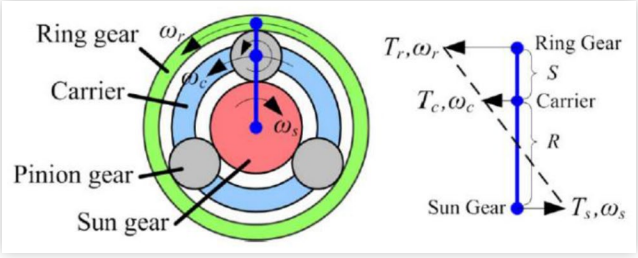

Each node can be connected to a powertrain component such as the engine, a motor, or a clutch. Kinematics of a PG set is governed by Equation 20.

$$\omega_s \cdot S + \omega_r \cdot R = \omega_c \cdot (R+S) \qquad \text{Eq. (20)}$$

where ω_r, ω_c, and ω_s denote the angular speeds of the ring gear, carrier, and sun gear, respectively. R and S refer to the radii of the ring gear and sun gear, respectively.

E. Complete Dynamics of AWD Power-Split Hybrid Powertrain

Given the component models, the dynamics of the rotational part for an AWD power-split hybrid design can be represented in a matrix form. To better illustrate the automated modeling technique, the lever diagram of the patented Toyota design with two output shafts is derived and used (excluding the automatic transmission), which is shown in Figure 9. The dynamic equations of this powertrain are shown in Equations 21 and 22, together with the battery dynamics in Equation 23, where $I_{(\cdot)}$ denotes the corresponding inertia and $F_{(\cdot)}$ denotes internal gear force of the corresponding PG set.

$$\begin{aligned}
&T_e + F_1(R_1+S_1) = \dot{\omega}_e(I_e + I_{c1})\\
&(-T_F) + F_2(R_2+S_2) = \dot{\omega}_F(I_F + I_{c2})\\
&T_{mg2} + (-T_R) + F_2(-S_2) = \dot{\omega}_R(I_R + I_{mg2} + I_{s2})\\
&T_{mg1} + F_1(-S_1) = \dot{\omega}_{mg1}(I_{mg1} + I_{s1})\\
&F_1(-R_1) + T_{cl1}\cdot 1 = \dot{\omega}_{r1}\cdot I_{r1}\\
&F_2(-R_2) + T_{cl1}\cdot(-1) = \dot{\omega}_{r2}\cdot I_{r2}
\end{aligned} \qquad \text{Eq. (21)}$$

FIGURE 9 Lever diagram of the Toyota AWD patent (excluding the automatic transmission) with significant forces and torques labeled. Reprinted with permission from Ref. [27].

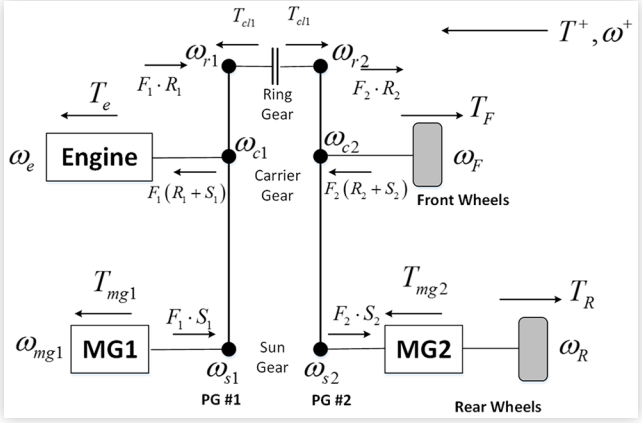

$$\begin{aligned}
&(R_1+S_1)\dot{\omega}_e = R_1\dot{\omega}_{r1} + S_1\dot{\omega}_{mg1}\\
&(R_2+S_2)\dot{\omega}_F = R_2\dot{\omega}_{r2} + S_2\dot{\omega}_{mg2}\\
&\dot{\omega}_{r1} - \dot{\omega}_{r2} = 0
\end{aligned} \qquad \text{Eq. (22)}$$

$$\dot{SOC} = -\frac{V_{oc} - \sqrt{V_{oc}^2 - 4R_{bat}P_{elect}}}{2\cdot R_{bat}} \qquad \text{Eq. (23)}$$

Equations 21 and 22 can be rearranged into the matrix representation shown in Equation 24.

$$\begin{bmatrix}
I_e+I_{c1} & 0 & 0 & 0 & 0 & 0 & R_1+S_1 & 0 & 0\\
0 & I_F+I_{c2} & 0 & 0 & 0 & 0 & 0 & R_2+S_2 & 0\\
0 & 0 & I_R+I_{mg2}+I_{s2} & 0 & 0 & 0 & 0 & -S_2 & 0\\
0 & 0 & 0 & I_{mg1}+I_{s1} & 0 & 0 & -S_1 & 0 & 0\\
0 & 0 & 0 & 0 & I_{r1} & 0 & -R_1 & 0 & 1\\
0 & 0 & 0 & 0 & 0 & I_{r2} & 0 & -R_2 & -1\\
R_1+S_1 & 0 & 0 & -S_1 & -R_1 & 0 & 0 & 0 & 0\\
0 & R_2+S_2 & -S_2 & 0 & 0 & -R_2 & 0 & 0 & 0\\
0 & 0 & 0 & 0 & 1 & -1 & 0 & 0 & 0
\end{bmatrix}
\cdot
\begin{bmatrix}
\dot{\omega}_e\\ \dot{\omega}_F\\ \dot{\omega}_R\\ \dot{\omega}_{mg1}\\ \dot{\omega}_{r1}\\ \dot{\omega}_{r2}\\ F_1\\ F_2\\ T_{cl1}
\end{bmatrix}
=
\begin{bmatrix}
T_e\\ -T_F\\ -T_R+T_{mg2}\\ T_{mg1}\\ 0\\ 0\\ 0\\ 0\\ 0
\end{bmatrix} \qquad \text{Eq. (24)}$$

In Equations 21 through 24, T_F and T_R imply the equivalent vehicle torques at front and rear wheels which can be expressed in Equations 25 and 26 based on Equations 14 and 15. Similarly, the equivalent front wheel inertia and rear wheel inertia can be shown in Equations 27 and 28.

$$T_F = \frac{\alpha}{\alpha+1}(Mar + T_{roll} + D_A) \qquad \text{Eq. (25)}$$

$$T_R = \frac{1}{\alpha+1}(Mar + T_{roll} + D_A) \qquad \text{Eq. (26)}$$

$$I_F = \frac{\alpha}{\alpha+1}(I_f + I_r) \qquad \text{Eq. (27)}$$

FIGURE 10 Patterns of the proposed matrix representation.

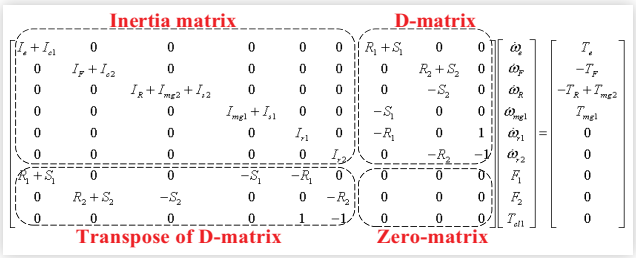

$$I_R = \frac{1}{\alpha+1}\left(I_f + I_r\right) \qquad \text{Eq. (28)}$$

It should be noted that in this power-split dynamics (Equation24) there are 14 variables to be determined using the 9 equations, given all the component inertias and PG ratios $R_1 : S_1$ and $R_2 : S_2$. Given a driving cycle to follow, ω_R and ω_F are determined; T_F and T_R are also determined when the front to rear torque ratio α is defined. The only free variable to be controlled is either the engine speed or engine torque.

The square matrix of the integrated dynamics shown in Equation 24 can be decomposed into four sub-matrices as shown in Figure 10. The components' and gears' inertias are assembled along the diagonal of the inertia matrix. The D-matrix is defined in Figure 10. It represents components connection and it is a unique mapping to a given design.

The automated modeling process to be described in the next section mainly involves generating the D-matrix systematically given the component connections and clutch states.

IV. Automated Modeling Process

The automated modeling process consists of two steps: 1) Initialize the configuration matrix of a design which shows the collocation of powertrain components excluding clutches; 2) Use clutch states to determine the dynamics.

A. Step 1 - Initialize the Configuration Matrix

An 8×8 zero matrix is first created, which is decomposed into four sub-matrices $\begin{bmatrix} J & D_{ini} \\ D_{ini}^T & 0 \end{bmatrix}$ where J is a 6×6 matrix and D_{ini} is a 6×2 matrix. The first four elements of the principal diagonal of J are replaced by the components' inertias in the order of engine, front output shaft, rear output shaft with MG2, and MG1.

PG set gear inertias are added to the principal diagonal of the sub-matrix J following their collocations with added components. For example, as indicated in the AWD patented design in Figure 9, the carrier of the first PG is collocated with the engine, so the first element in the principal becomes $I_e + I_{c1}$. The last two diagonal entries of the sub-matrix J are filled with the remaining gear inertias.

The upper-right 6×2 sub-matrix D_{ini} has 2 columns which are determined by the number of PGs in this design. Entries of this sub-matrix are determined by the collocation between the PG set nodes and components. When a powertrain component is connected to a PG node, the "node coefficient" will be $-S_{(\cdot)}$ if it is connected to the sun gear, $-R_{(\cdot)}$ if it is connected to the ring gear, and $S_{(\cdot)} + R_{(\cdot)}$ if it is connected to the carrier. By defining the corresponding (external) component torque vector T_{ini} and angular acceleration vectors $\dot{\Omega}_{ini}$, the following matrices are assembled, together with the battery dynamics:

$$J = \begin{bmatrix} I_e + I_{c1} & 0 & 0 & 0 & 0 & 0 \\ 0 & I_F + I_{c2} & 0 & 0 & 0 & 0 \\ 0 & 0 & I_R + I_{mg2} + I_{S2} & 0 & 0 & 0 \\ 0 & 0 & 0 & I_{mg1} + I_{s1} & 0 & 0 \\ 0 & 0 & 0 & 0 & I_{r1} & 0 \\ 0 & 0 & 0 & 0 & 0 & I_{r2} \end{bmatrix}$$

$$D_{ini} = \begin{bmatrix} R_1 + S_1 & 0 \\ 0 & R_2 + S_2 \\ 0 & -S_2 \\ -S_1 & 0 \\ -R_1 & 0 \\ 0 & -R_2 \end{bmatrix}$$

$$T_{ini} = \begin{bmatrix} T_e & (-T_F) & (-T_R) + T_{mg2} & T_{mg1} & 0 & 0 & 0 & 0 \end{bmatrix}^T$$

$$\dot{\Omega}_{ini} = \begin{bmatrix} \dot{\omega}_e & \dot{\omega}_F & \dot{\omega}_R & \dot{\omega}_{mg1} & \dot{\omega}_{r1} & \dot{\omega}_{r2} & F_1 & F_2 \end{bmatrix}^T$$

$$P_{elect} = T_{MG1}\omega_{MG1}\eta_{MG1}^{k1} + T_{MG2}\omega_{MG2}\eta_{MG2}^{k2}$$

$$\dot{SOC} = -\frac{V_{oc} - \sqrt{V_{oc}^2 - 4R_{bat}P_{elect}}}{2 \cdot R_{bat}} \qquad \text{Eq. (29)}$$

B. Step 2 - Use Clutch States to Obtain the Dynamics

Whenever there is a clutch connection, the sub-matrix D_{ini} will be augmented with a zero column. The corresponding two entries of this augmented column, which indicates connection of two PG nodes, are then replaced with 1 and –1.

The same procedure applies to D_{ini}^{T}. The sub-matrix D_{ini} is then augmented and referred as matrix D. It should be noticed that the augmented elements 1 and -1 indicate those two nodes sharing the same rotational speed and acceleration. In the given example, they indicate the coefficients of the relationship $(1)\cdot\dot{\omega}_{r1}+(-1)\cdot\dot{\omega}_{r2}=0$.

The clutch addition also augments $\dot{\Omega}_{ini}$ and T_{ini}. When a clutch connection is added, $\dot{\Omega}_{ini}$ is augmented with an element $T_{cl(\cdot)}$, which represents the internal torque on this added connection/clutch. T_{ini} is augmented with a zero, which represents zero external torque directly on this internal connection. The augmented $\dot{\Omega}_{ini}$ and T_{ini} are denoted as $\dot{\Omega}$ and T.

By defining the augmented matrix as the A matrix, the complete dynamics of the referred Toyota patented design (in Figure 9) is shown in Equation 30, together with the augmented sub-matrix D in Equation 31. It can be noticed that Equation 30 is the matrix representation of the dynamics derived in Equations 21 through 23. Those filled entries, such as $-S_{(\cdot)}$, $-R_{(\cdot)}$, 1 and −1, determine the internal forces/torques acting on the corresponding nodes.

$$A=\begin{bmatrix} I_e+I_{c1} & 0 & 0 & 0 & 0 & 0 & R_1+S_1 & 0 & 0 \\ 0 & I_F+I_{c2} & 0 & 0 & 0 & 0 & 0 & R_2+S_2 & 0 \\ 0 & 0 & I_R+I_{mg2}+I_{s2} & 0 & 0 & 0 & 0 & -S_2 & 0 \\ 0 & 0 & 0 & I_{mg1}+I_{s1} & 0 & 0 & -S_1 & 0 & 0 \\ 0 & 0 & 0 & 0 & I_{r1} & 0 & -R_1 & 0 & 1 \\ 0 & 0 & 0 & 0 & 0 & I_{r2} & 0 & -R_2 & -1 \\ R_1+S_1 & 0 & 0 & -S_1 & -R_1 & 0 & 0 & 0 & 0 \\ 0 & R_2+S_2 & -S_2 & 0 & 0 & -R_2 & 0 & 0 & 0 \\ 0 & 0 & 0 & 0 & 1 & -1 & 0 & 0 & 0 \end{bmatrix}$$

$$T=\begin{bmatrix} T_e & (-T_F) & (-T_R)+T_{mg2} & T_{mg1} & 0 & 0 & 0 & 0 & 0 \end{bmatrix}^T$$

$$\dot{\Omega}=\begin{bmatrix} \dot{\omega}_e & \dot{\omega}_F & \dot{\omega}_R & \dot{\omega}_{mg1} & \dot{\omega}_{r1} & \dot{\omega}_{r2} & F_1 & F_2 & T_{cl1} \end{bmatrix}^T$$

$$P_{elect}=T_{MG1}\omega_{MG1}\eta_{MG1}^{k1}+T_{MG2}\omega_{MG2}\eta_{MG2}^{k2}$$

$$S\dot{O}C=-\frac{V_{oc}-\sqrt{V_{oc}^2-4R_{bat}P_{elect}}}{2\cdot R_{bat}} \qquad \text{Eq. (30)}$$

$$D=\begin{bmatrix} R_1+S_1 & 0 & 0 \\ 0 & R_2+S_2 & 0 \\ 0 & -S_2 & 0 \\ -S_1 & 0 & 0 \\ -R_1 & 0 & 1 \\ 0 & -R_2 & -1 \end{bmatrix} \qquad \text{Eq. (31)}$$

Grounding clutch/brake connections can be added under similar manner by having 1 in the corresponding node entry. The augmented element 1 indicates the connected node has the zero rotational speed and acceleration. For example, if the ring gear node of the first PG is grounded, the coefficients of the relationship are indicated as $(1)\cdot\dot{\omega}_{r1}=0$.

For all designs similar to Figure 4 but allowing different configurations and three clutches, assuming MG1 and MG2 are identical, the total number of possible designs is $0.5\cdot P_6^4\cdot C_{15}^3=180\cdot 455=81900$. Details of calculating this number can be found in the Appendix. The number of design candidates becomes 18,427,500, when considering the PG gear ratio varies from 2:1 to 4:1, and final drive ratio varies between 2:1 and 6:1 (both with step size 1).

V. Systematic Screening Process

The following three attributes to be checked are desired when designing AWD hybrid pickup trucks:

- *All-wheel drive (AWD)*: the engine can provide positive torque at both output shafts.
- *All-wheel regenerative braking (AWRB)*: the two electric motors can provide desired negative torque at both output shafts.
- *Driving backward using engine power*: the engine can have effective negative torque at the output shaft(s) when the vehicle drives backwards (the output shaft speeds are negative).

The AWD attribute ensures a truck design's towing and grade performance; the AWRB attribute ensures better regenerative braking performance; and the driving backward using engine power attribute ensures the hybrid truck can sustain when backing up a towed load on a slope even when the battery SOC is low.

Besides those desired attributes, the performance criteria are also specified: Vehicle top speed must be at least 90 mph. The average acceleration from 0 to 60 mph must be higher than 3.6m/s^2. These two criteria ensure that the obtained designs are competitive against the benchmark (the conventional, non-hybrid vehicle). It should be noticed that the desired criteria is not limited to the given two and can be specified by designer's request such as gradeability. For a case study, the top speed and 0–60 mph acceleration are highlighted.

A. Performance Attributes Screening

Given the complete dynamics in Equation 30, the $\dot{\Omega}$, which contains the nodes' accelerations and internal torques/forces, can be expressed in Equation 32 by inversing Equation 30.

TABLE 4 Performance attribute screening rules.

Desired attributes	Screening condition
AWD	$A_{inv21} > 0$, $A_{inv31} > 0$
AWRB	$A_{inv24} \neq 0$, $A_{inv21} = 0$, $A_{inv31} = 0$
Driving backward using engine power	$A_{inv21} < 0$, $A_{inv31} < 0$

$$\dot{\Omega} = A^{-1} \cdot T$$

$$A^{-1} = \begin{bmatrix} A_{inv11} & A_{inv12} & A_{inv13} & A_{inv14} & A_{inv15} & \cdots & \cdots \\ A_{inv21} & \cdots & \cdots & & & & \cdots \\ A_{inv31} & \cdots & & & & & \\ A_{inv41} & & & & & & \\ A_{inv51} & & & & & & \\ A_{inv61} & & & & & & \\ \cdots & & & & & & \\ & & & & & & \\ \cdots & \cdots & & & & & \cdots \end{bmatrix}$$

$$T = \begin{bmatrix} T_e & (-T_F) & (-T_R)+T_m & T_g & 0 & 0 & 0 & 0 & 0 \end{bmatrix}^T$$

$$\dot{\Omega} = \begin{bmatrix} \dot{\omega}_e & \dot{\omega}_F & \dot{\omega}_R & \dot{\omega}_g & \dot{\omega}_{r1} & \dot{\omega}_{r2} & F_1 & F_2 & T_{cl1} \end{bmatrix}$$

$$P_{elect} = T_{MG1}\omega_{MG1}\eta_{MG1}^{k1} + T_{MG2}\omega_{MG2}\eta_{MG2}^{k2}$$

$$\dot{SOC} = -\frac{V_{oc} - \sqrt{V_{oc}^2 - 4R_{bat}P_{elect}}}{2 \cdot R_{bat}} \qquad \text{Eq. (32)}$$

Then, elements in the A^{-1} matrix are used for attribute screening according to the rules summarized in Table 4.

Note that A_{inv21}^{-1} and A_{inv31}^{-1} relate engine torque with the front output and rear output, respectively. A_{inv24}^{-1} relates MG1 torque with the front output.

B. Performance Criteria Screening

To perform the performance screening in a computationally efficient manner, we focus on torque relationships (system kinetics) extracted from the complete dynamics (30) – (32) and neglect other components' inertias except for the vehicle inertias. The front-wheel acceleration and rear-wheel acceleration are assumed to be the same. The torque relationships of all six PG nodes are obtained from the first six rows (six-system kinetics) of the dynamics $A\dot{\Omega} = T$ through the sub-matrix D. Taking the referred Toyota patent [28] in Figure 9 as an example again, the relationships are obtained in Equation 33 by neglecting the gear inertias, engine inertia, and motor inertias. Notice that the last two elements of the torque vector in Equation 32 are zeros after neglecting the gear inertias.

$$D\begin{bmatrix} F_1 \\ F_2 \\ T_{cl1} \end{bmatrix} = \begin{bmatrix} T_e \\ (-T_F)+(-I_F \cdot \dot{\omega}_F) \\ (-T_R)+(-I_R \cdot \dot{\omega}_R)+T_{mg2} \\ T_{mg1} \\ 0 \\ 0 \end{bmatrix} \qquad \text{Eq. (33)}$$

Considering the torque relationships in Equation 33, the best average acceleration rate $\bar{a}$ of each design can be calculated by Equations 34 and 35 and used to estimate the launching performance. To complete the calculation for the best possible acceleration, vehicle speed grid n and the targeted speed v_{tar} = 60 mph are used.

The maximum acceleration at the ith grid point is calculated in Equation 34 based on the maximum combined output torque from Equation 33. R_{tire} is the tire radius, and FR is the final drive gear ratio. T_{vmax} refers to the maximum output torque at the vehicle. T_{F_trac} and T_{R_trac} refer to the traction output torque at the front wheels and rear wheels, respectively. μ_{tire} is the tire-road friction coefficient and is 0.8 in our study.

All combinations of T_e, T_{MG1}, and T_{MG2} are used to calculate the summation of T_{F_trac} and T_{R_trac} through Equation 33. T_{vmax} are the maximum values obtained. Details in calculating the acceleration can be found in the Appendix.

$$\begin{aligned} a_i &= \frac{T_{v\max}}{I_v} \cdot \frac{R_{tire}}{FR} \\ T_{v\max} &= \max\left(T_{F\_trac} + T_{R\_trac}\right) \\ T_{F\_trac} &= -T_F - I_F \cdot \dot{\omega}_F \\ T_{R\_trac} &= -T_R - I_R \cdot \dot{\omega}_F \\ I_v &= I_F + I_R \\ \dot{\omega}_v &= \dot{\omega}_F = \dot{\omega}_R = a_i \cdot R_{tire} \\ T_{F\max} &\le N_{z_f} \cdot \mu_{tire} \\ T_{R\max} &\le N_{z_r} \cdot \mu_{tire} \end{aligned} \qquad \text{Eq. (34)}$$

$$\bar{a} = \frac{n}{\sum_1^n \frac{1}{a_i}} \qquad \text{Eq. (35)}$$

The threshold to screen for the average acceleration $\bar{a}$ can use the criteria of launching acceleration time from the SAE Standard J2807 [10] or the acceleration rate of the competitive benchmark (non-hybrid) vehicle.

All these requirements for desired attributes and criteria not only screen for competent designs but they also substantially reduce the size of the feasible design pool as a more efficient design search strategy.

For the following case study, three performance attributes are used for the case study: AWD, AWRB, and AWD Backward

Using Engine Power. The performance of the conventional (non-hybrid) F-150 vehicle, which is more aggressive than the SAE Standard J2807, is used as the design requirement. With the defined requirements, 6 designs with 328 different gear sizing (i.e., PG gear ratio and final drive ratio) combinations survive the screening.

VI. Evaluations for Acceleration Performance and Fuel Economy

For all surviving design candidates, comparison must use results with optimal or near-optimal control to ensure fairness. For evaluating acceleration, DP is used to obtain the theoretically best launching performance. For evaluating fuel economy, although DP guarantees global optimality, it is sometimes impractical to use due to its high computational cost resulted from the curse of dimensionality. In a large-scale design search, it may take months or even years to finish the exhaustive search. The PEARS method in [20] employs a near-optimal energy management that is ten thousand times faster than the DP while it delivers near-optimal results. In this article, we adapt the PEARS method with DP to solve control problem for AWD multi-mode power-split hybrid powertrains.

A. Acceleration Performance Evaluation

The objective of this evaluation step is to find the control inputs that accelerate the vehicle to reach the targeted speed. The control problem is then an optimization problem for at each time step as shown in Equation 36.

$$\begin{aligned} \max \quad & a(k) \\ s.t. \quad & v(k) = \sum_{i=1}^{k} a_{\max}(i) \cdot \Delta t + v_0 \\ & t(k) = k \cdot \Delta t \\ & v_0 = 0 \\ & v(k) \le v_{target} \\ & \forall k \in 1,2,\ldots,N \end{aligned} \qquad \text{Eq. (36)}$$

The target speed v_{target} is 60 mph. Step size is $\Delta t = 0.1s$. $v(k)$ is the vehicle speed at time step k, and $a(k)$ is calculated from

$$a(k) = \dot{\omega}_r r = \dot{\omega}_f r \qquad \text{Eq. (37)}$$

The optimization problem is solved through brute force search, by examining all combinations of T_e, T_{MG1}, and T_{MG2} to obtain the maximum acceleration. This free-terminal-time optimization continues until the vehicle speed reaches 60 mph. Battery SOC constraint is not considered, because the 0 – 60 mph launching action only lasts for a very short time.

B. Fuel Economy Evaluations Using the Power-Weighted Efficiency Analysis for Rapid Sizing Method

The fuel economy evaluation is formulated as a control optimization problem to minimize the fuel consumption given a desired drive cycle as follows:

$$\begin{aligned} \min \quad & J = \sum_{k=0}^{N-1} \dot{m}_f(f) \\ & \dot{\Omega} = A^{-1} \cdot T \\ s.t. \quad & \dot{SOC} = f_{bat}(P_{bat}) \\ & \dot{m}_f = f_e(\omega_e, T_e) \\ & \underline{x} \le x_k \le \bar{x}, \forall k \\ & \underline{u} \le x_k \le \bar{u}, \forall k \end{aligned} \qquad \text{Eq. (38)}$$

$\dot{m}_f$ is the engine fuel rate; $\dot{\Omega} = A^{-1}T$ is the inverse complete dynamics in Equations 30 and 31; $\dot{SOC}$ represents the battery dynamics; f_e represents the engine fuel model shown in Figure 6; N is the problem horizon length; k represents the time step; x represents all the states; u represents all the controls; and the rest are the constraints of states and controls. For the design optimization problem for the modeled AWD multi-mode power-split hybrid powertrains, there are three controls (operating mode, engine torque, and MG2 torque) and two states (engine speed and battery SOC).

The PEARS method is incorporated into the above optimization problem in Equation 38. It is a near-optimal energy management methodology which was originally designed for component sizing, and used here to simplify the optimization problem. The PEARS method introduces a power-weighted efficiency η_{Hybrid}, which relates the fuel consumption and battery SOC, and pre-maximizes this efficiency for each operating mode.

For implementation, the PEARS method first analyzes the target cycle by discretizing the driving cycle in two dimensions: vehicle speed and vehicle torque demand. It then uses the discretized information to optimize the control input for all the operating modes based on the defined power-weighted efficiency. The process of PEARS with DP method is summarized in Figure 11.

For electric vehicle (EV) modes, electric motor powers P_{MG1} and P_{MG2} are obtained given a combination of the rear-to-front torque ratio α as well as their corresponding torques. Subsequently, the loss in electrical system P_{EV}^{loss} and battery

FIGURE 11 The process of PEARS with DP method [20].

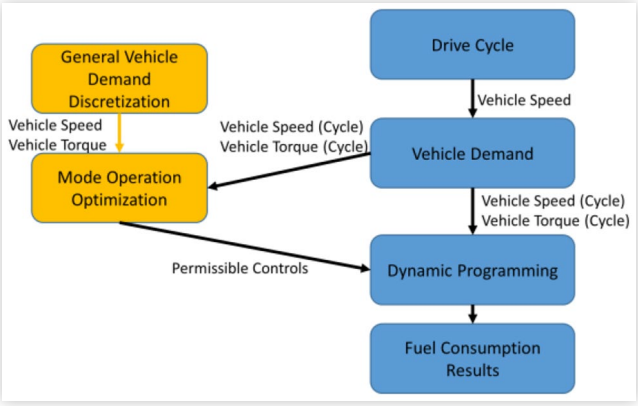

power P_{EV}^{in} can be calculated. Then, the best possible efficiency for an EV mode is obtained from Equations 39 and 40.

$$\eta_{EV} = 1 - \frac{P_{EV}^{loss}}{P_{EV}^{in}} \quad \text{Eq. (39)}$$

$$\eta_{EV}^{*}\Big|_{v,a} = \max\left[\eta_{EV}\left(\alpha, T_{MG1}, T_{MG2}\right)\right]\Big|_{v,a} \quad \text{Eq. (40)}$$

For hybrid modes, four power flows P_{e_1}, P_{e_2}, P_{e_3}, and P_{batt} are defined, as shown in Table 5. Similar to the EV mode analysis, by examining all combinations of rear-to-front torque ratio, speed and torque, the highest power-weighted efficiency is defined and calculated in Equations 41 and 42.

$$\eta_{Hybrid}\left(\alpha, \omega_e, T_e\right) = \frac{P_{e\_1}\eta_G\eta_{batt} / \left(\eta_{e\_\max}\eta_{G\_\max}\right)}{P_{fuel} + \mu P_{batt}} + \frac{P_{e\_2}\eta_G\eta_M / \left(\eta_{e\_\max}\eta_{G\_\max}\eta_{M\_\max}\right)}{P_{fuel} + \mu P_{batt}} + \frac{P_{e\_3} / \eta_{e\_\max} + \mu P_{batt}\eta_{batt}\eta_M / \eta_{M\_\max}}{P_{fuel} + \mu P_{batt}} \quad \text{Eq. (41)}$$

$$\eta_{Hybrid}^{*}\Big|_{v,a} = \max\left[\eta_{Hybrid}\left(\alpha, \omega_e, T_e\right)\right]\Big|_{v,a} \quad \text{Eq. (42)}$$

TABLE 5 Power-flow of the hybrid system.

Power flow	Description
P_{e_1}	Engine power that goes through the generator
P_{e_2}	Engine power that goes through generator to motor
P_{e_3}	Engine power that directly flows to the final drive
P_{batt}	Battery power that drives the motor

In Equations 41 and 42, η_G, η_M, and η_{batt} refer to the efficiency of generator, motor, and battery, respectively. P_{fuel} refers to engine power, and μ is a flag to indicate whether the battery assist is on or not. The power-weighted efficiency η_{Hybrid} relates the fuel and battery cost for the multi-object optimization. Moreover, the fuel consumption $f_{e,opt}$ of each optimized mode is also obtained. Then, the efficiency is used to pre-optimize the control and reduce the space of the control problem, so that DP becomes possible for evaluation for a large amount of design candidates.

For each operating mode represented by the dynamics developed in Equation 30, given a driver demand (vehicle torque and vehicle speed), the power-weighted efficiency η_{Hybrid}* is maximized by searching for all possible engine torque, MG2 torque, and engine speed. This is repeated for all driver demands and the optimal cost relationship is generated shown in Equation 43.

$$\dot{m}_{f,C} = f_{e,opt}\left(\omega_v, T_v, C\right) \quad \text{Eq. (43)}$$

This optimization problem for multi-mode AWD power-split hybrid vehicles is then simplified to 1 control (operating mode) and 1 state (battery SOC). Then, DP becomes possible to be implemented to solve the optimization problem for a drive cycle. The optimization is then simplified and shown in Equation 44, where C is the mode selection as the control to the optimization.

$$\begin{aligned} \min \quad & J = \sum_{k=0}^{N-1} \dot{m}_{f,C}(k) \\ s.t. \quad & \dot{m}_{f,C} = f_{e,opt}\left(\omega_v, T_v, C\right) \\ & \dot{SOC} = f_{bat}\left(P_{bat}\right) \\ & \dot{\Omega} = A_C^{-1} \cdot T \\ & SOC_{\min} \le SOC \le SOC_{\max} \\ & C \in \text{Operating Mode} \end{aligned} \quad \text{Eq. (44)}$$

VII. Optimization Results

In this article, a conceptual Ford F-150 is chosen for the case study of pickup trucks. Comparisons are among the conventional F-150, a pre-transmission parallel hybrid F-150 (shown in Figure 12), and AWD hybrid F-150. Key

FIGURE 12 Schematic of the pre-transmission parallel hybrid design benchmark.

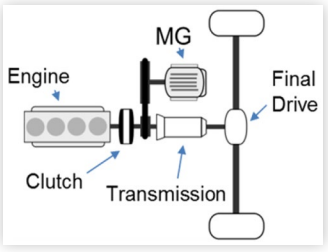

TABLE 6 Parameters of the vehicle used in the case study (F-150).

Component vehicle	Conventional	Parameters parallel	AWD hybrid
Engine	272 kw@ 5200rpm 569 Nm@ 2500rpm	272 kw@ 5200rpm 569 Nm@ 2500rpm	163-272 kw@5200rpm
MG1 power	N/A	90 kW	66-110 kW
MG2 power	N/A	N/A	66-110 kW
Transmission	6-speed	6-speed	2-PG set
Drivetrain	RWD	RWD	AWD

powertrain parameters are summarized in Table 6. The powertrain components' design pool includes three power sizes for engine (163 kW, 217 kW, and 272 kW) and three power sizes for the two electric motors (66 kW, 88 kW, and 110 kW). It should be mentioned that candidate sizes of motor(s) and the engine can vary based on the design request. In this case study, an electric motor is assumed to be collocated with the rear output shaft; however, the proposed design methodology can be applied to other scenarios easily.

Combined results of launching performance and fuel economy of the feasible design candidates are shown in Figure 13. There is a family of designs achieving both better acceleration and better fuel economy than the conventional and the parallel hybrid vehicles. Two winning designs (design *A* and design *B*) are highlighted in Figures 14 and 15. Both of them have a large number of design candidates (i.e., design with different components' size combinations) showing excellent results in a performance metric of 0-60 acceleration and fuel economy.

An optimal design candidate from design *A* is selected for further analysis with its powertrain component sizes

FIGURE 13 Combined performance and fuel economy results for various hybrid design candidates.

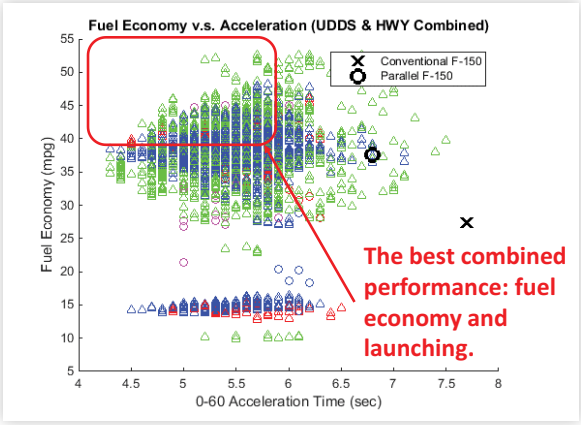

FIGURE 14 Drawing of design *A*.

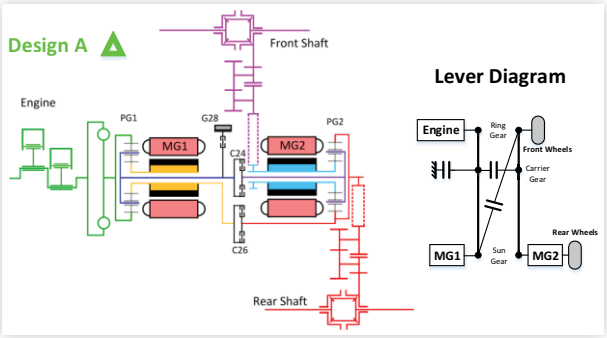

FIGURE 15 Drawing of design *B*.

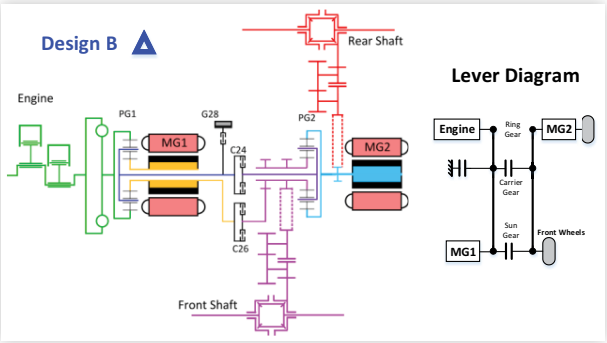

shown in Table 7. This highlighted design has the same maximum system power (362 kW) as the benchmark parallel hybrid design. Performance results comparison with the conventional and parallel design is summarized in Table 8. Selected performance results are shown in Figures 16 and 17.

TABLE 7 Powertrain parameters of design *A*.

Engine	MG1	MG2	R/S ratio (PG1)	R/S ratio (PG2)	Final drive (Front)	Final drive (Rear)
163 kW	110 kW	88 kW	2:1	4:1	5:1	6:1

TABLE 8 Performance summary.

Vehicle	Launching time (sec) (16,000 lbs.)	Launching time (sec) (5073 lbs).	Fuel economy – UDDS (mpg) (5073 lbs).	Fuel economy – HWFET (mpg) (5073 lbs).
Conventional	21.6	7.7	25.0	30.3
Parallel	17.3	7.1	42.3	31.7
AWD winning design *A*	13.5	5.1	50.0	34.8

FIGURE 16 0-to-60 launching performance results.

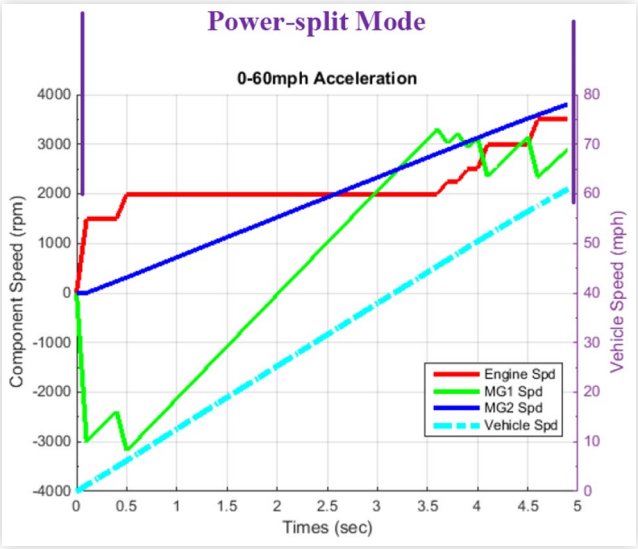

FIGURE 18 0-to-60 launching performance comparison between AWD winning design and RWD parallel example.

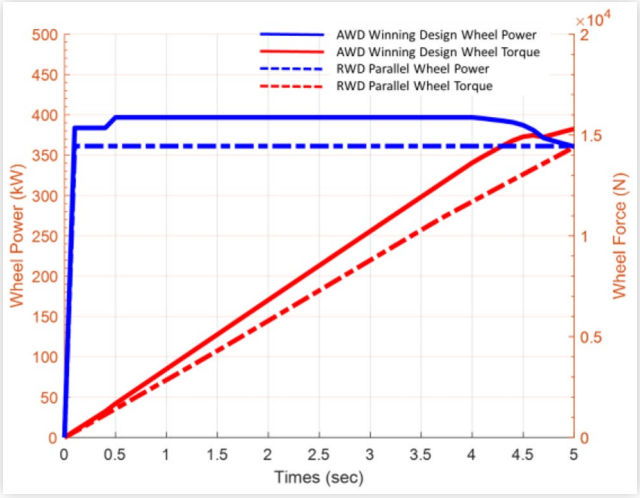

Figure 16 shows how the highlighted winning design accelerates from 0 to 60 mph. The power-split mode is used to achieve the best launching in 5.1 s. It controls the engine speed for maximum engine torque. The 0-60 acceleration performance comparison between the AWD winning design and RWD parallel example is shown in Figure 18.

The winning design *A* shows 28% faster in launching, and 18.2% and 9.8% better fuel economy on UDDS and HWY cycle, respectively. Results from the two drive cycles are shown in Figure 17. The regenerative braking energy analysis for both cycles is shown in Table 9. The superior performance over the parallel hybrid F-150 design indicates that this systematic design methodology successfully identifies a family of good AWD designs.

VIII. Analysis of the Highlighted AWD Hybrid Power-Split Vehicle Designs

A. Common Features of the Two Winning Designs

It is observed that the two highlighted designs (Design *A* and Design *B*) share several common features. Each design

FIGURE 17 Simulation results for UDDS and HWFET drive cycles.

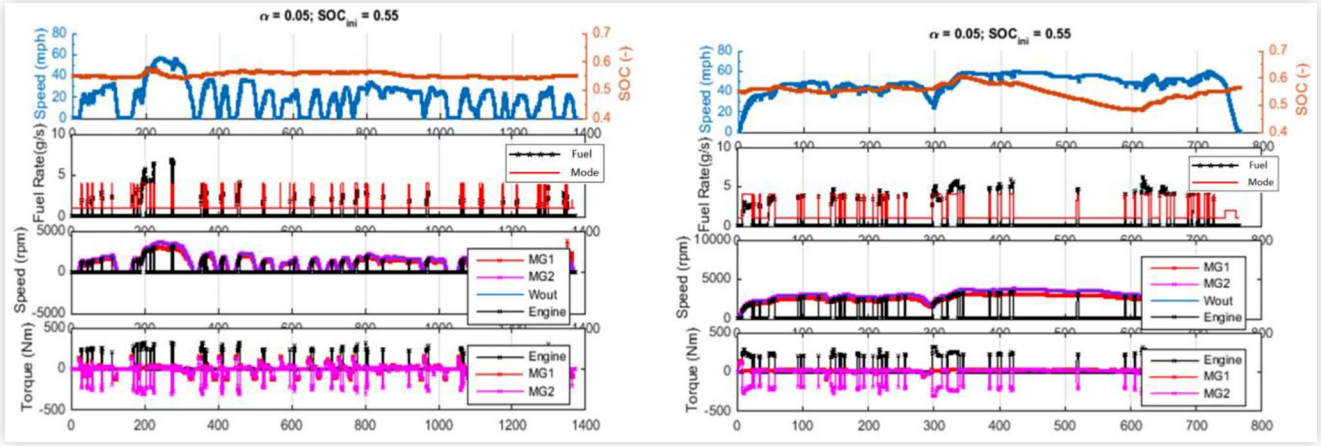

TABLE 9 Regenerative braking energy analysis.

Drive cycle	UDDS	HWFET
Required energy (J)	$1.33 \cdot 10^7$	$9.09 \cdot 10^6$
Regenerative braking energy (J)	$-2.75 \cdot 10^6$	$-8.36 \cdot 10^5$
Regen energy percentage	20.7%	9.20%

has a clutch connecting the carrier nodes of the two PG sets. The two output shafts are on the same PG set, connecting to the sun gear node and the ring gear node. These common features allow a good torque balance of the second PG set.

B. Fuel-Saving Control Policy from Optimization Results

From the results under the two driving cycles, it was observed that the EV mode and parallel mode are used most: the parallel mode is used in high power driving and the EV mode is used for low power driving and during braking. To better understand this observation, the mode distribution is shown in Figure 19. The two operating modes are also shown in Figure 20.

Based on the observation from 0 to 60 launching (when power-split mode is used) and the fuel-efficient driving in EPA cycles, a policy for mode selection is generated and shown in Figure 21. While this mode selection map is very simple and

FIGURE 19 Operation mode analysis for UDDS and HWY cycles.

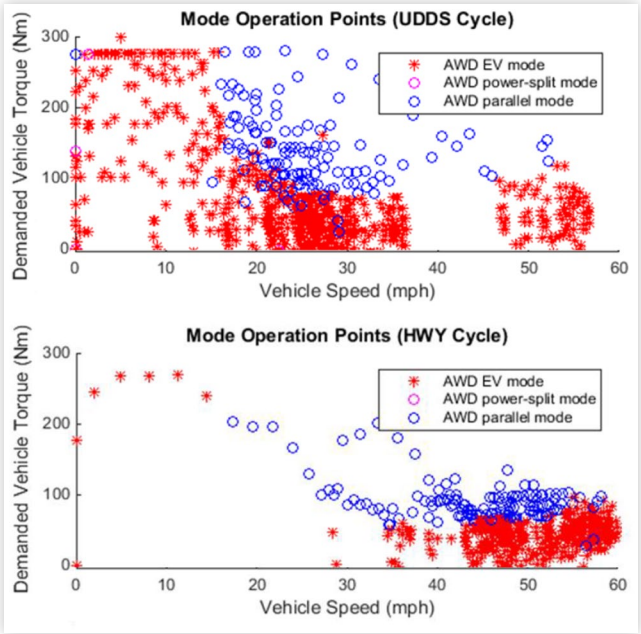

FIGURE 20 Lever diagram of EV mode and parallel mode.

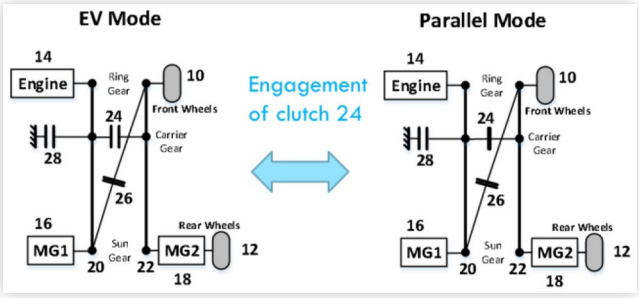

may lose some optimality, it summarizes from optimal control results and is implementable.

C. Comparison of Launching Performance and Gradeability for *AWD*, *FWD* Hybrid Vehicles and RWD Hybrid Vehicles

To better understand the performance of the highlighted AWD hybrid design, the acceleration and grade performance is shown and analyzed in this subsection. Two tests are designed based on the tow-vehicle propulsion requirements from the SAE Standard J2807. The AWD hybrid design, a FWD parallel design, and a RWD parallel design are compared with the same gross combination weight rating (GCWR) of 16000 lbs. The vehicle dynamics of the AWD design can be found in the Appendix.

Test 1 - Launch on 12% grade: time for launching the towing vehicle from 0 to 10 mph on a 12% grade.

Test 2 - Gradeability test: maximum grade on a slope while maintaining the vehicle speed at 40 mph.

FIGURE 21 Policy for typical mode selection.

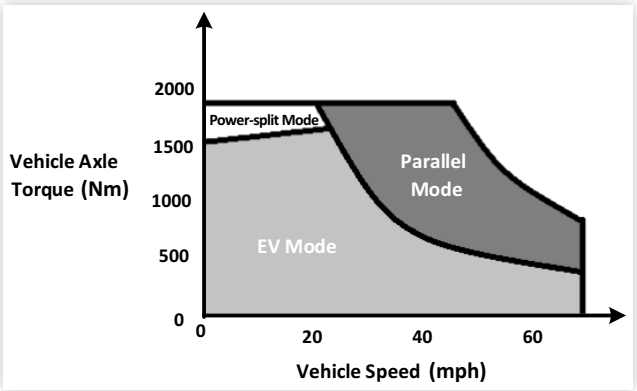

TABLE 10 Performance of launch on 12% grade and gradeability.

Vehicle (GCWR: 16000 lbs.)	Launch on 12% grade	Gradeability (at 40 mph)
FWD parallel	Infeasible	9.2%
RWD parallel	7.3 s	13.2%
AWD winning design #1	5.3 s	20.5%

From results shown in Table 10, the AWD power-split hybrid design is able to accelerate from 0 to 10 mph in 5.3 seconds, while the RWD parallel design needs 7.3 seconds to launch, and the FWD parallel design cannot even launch on the 12% grade slope. The AWD design can launch on a slope 55% steeper than the RWD parallel design can. The RWD design performs better than the FWD design does because of the vehicle load transfer. The AWD power-split hybrid design performs the best.

Figure 22 demonstrates the gradeability of these three designs by showing tow-weight capability on different slopes. The AWD hybrid design can tow heavier weight because it uses both axles. The FWD design tows even less than the RWD design because of load transfer. It is unable to drive the vehicle on a slope with 11% grade or higher at fully loaded weight.

IX. Summary

This article highlights the AWD multi-mode power hybrid vehicles for pickup trucks with superior performance on 0-60 acceleration and fuel economy, as well as other desired performance. It presents a systematic design methodology for this powertrain class in four steps. This systematic procedure screens out infeasible and incapable designs, thus it reduces the computation effort efficiently and makes it possible for large-scale design applications. All possible designs are modeled and examined exhaustively, and a family of optimal designs is able to be identified in this process. This design methodology is implemented in a case study on a conceptual Ford F-150 design. Six AWD multi-mode hybrid designs were found, and 328 candidates (with different gear sizing) were obtained that achieve better fuel economy and better launching performance compared to the conventional benchmark. All these designs achieve desired attributes including AWD, all-wheel regenerative braking, and driving backward using the engine power. The best design candidate achieves 28% faster launching, and 18.2% and 9.8% better fuel economy on UDDS and HWY cycles compared to the parallel hybrid design, while using the same total system power. It shows that the AWD power-split hybrid truck design can provide good fuel economy while satisfying the stringent launching, towing, and grade requirement.

FIGURE 22 Gradeability performance (at 40 mph) of the three designs.

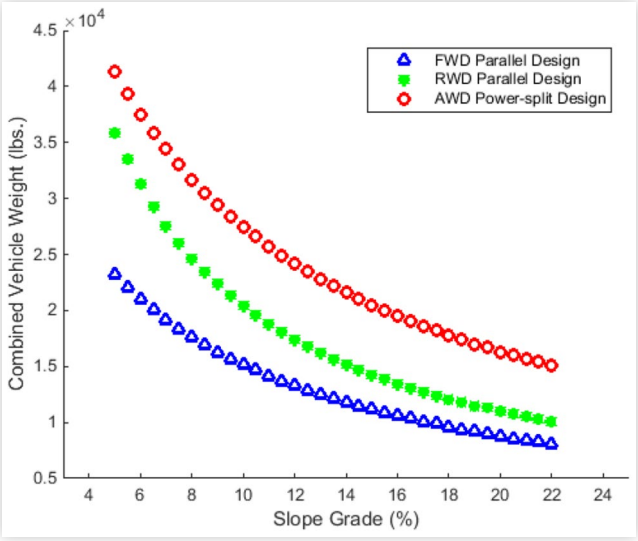

Acknowledgment

This work is supported by a grant from the Bosch Energy Research Network. Obtained optimal AWD power-split designs have been submitted for patent applications. Inherited from the design methodology shown in this article, the author is currently working on the U.S. Department of Energy (DOE) funded project (FOA#: DE-FOA-0001349) and building a prototype power-split multi-mode hybrid powertrain for truck applications.

This article is an extended, modified version of the article "Optimal design of all-wheel-drive hybrid pick-up trucks" published by ASME 2015 Dynamic Systems and Control Conference (DSCC) [1]. Updated and modified with permission granted by ASME.

References

1. Pan, Z., Zhang, X., Silvas, E., Peng, H. et al., "Optimal Design of All-Wheel-Drive Hybrid Pick-Up Trucks," in *ASME 2015 Dynamic Systems and Control Conference*, Columbus, OH, 2015.
2. Environmental Protection Agency (EPA) and National Highway Traffic Safety Administration (NHTSA),"2017 and Later Model Year Light-Duty Vehicle Greenhouse Gas Emissions and Corporate Average Fuel Economy Standards; Final Rule,"2012, DOT. [Online]. Available: http://www.nhtsa.gov/fuel-economy.
3. Pawlowski, A. and Splitter, D., "SI Engine Trends: A Historical Analysis with Future Projections," SAE Technical Paper 2015-01-0972, 2015, doi:10.4271/2015-01-0972.
4. Abdelhamid, M., Haque, I., Pilla, S., Filipi, Z.S. et al., "Impacts of Adding Photovoltaic Solar System On-Board to Internal Combustion Engine Vehicles Towards Meeting 2025

Fuel Economy CAFE Standards," *SAE Int. J. Alt.Power.* 5(2):237-248, 2016, doi:10.4271/2016-01-1165.

5. Moawad, A. and Rousseau, A., "Impact of Electric Drive Vehicle Technologies on Fuel Efficiency to Support 2017-2025 CAFE Regulations," *SAE Int. J. Alt. Power* 3(2):163-175, 2014, doi:10.4271/2014-01-1084.
6. Lee, S., Cherry, J., Safoutin, M., Neam, A. et al., "Modeling and Controls Development of 48 V Mild Hybrid Electric Vehicles," SAE Technical Paper 2018-01-0413, 2018, doi:10.4271/2018-01-0413.
7. United States Environmental Protection Agency, "Fuel Economy Guide-Model Year 2018,"2018[Online]. Available: https://www.fueleconomy.gov/.
8. Kutz, M., *Environmentally Conscious Transportation*. Vol. 5 (John Wiley & Sons, 2008).
9. Csere, C., "2016 Toyota RAV4 Hybrid,"2015, Available: http://www.caranddriver.com/reviews/2016-toyota-rav4-hybrid-firstdrive-review.[Online.Accessed 2016].
10. SAE, "Performance Requirements for Determining Tow-Vehicle Gross Combination Weight Rating and Trailer Weight Rating,"Society of Automotive Engineers International, SAE Standard J2807, 2012.
11. Keulen, T.V., Mullem, D.V., Jager, B.D., Kessels, J.T. et al., "Design, Implementation, and Experimental Validation of Optimal Power Split Control for Hybrid Electric Trucks," *Control Engineering Practice* 20(5):547-558, 2012.
12. Filipi, Z., Louca, L., Daran, B., Lin, C.C. et al., "Combined Optimisation of Design and Power Management of the Hydraulic Hybrid Propulsion System for the 6 × 6 Medium Truck," *International Journal of Heavy Vehicle Systems* 11:372-372, 2004.
13. Li, C.-T. and Peng, H., "Optimal Configuration Design for Hydraulic Split Hybrid Vehicles," *American Control Conference (ACC)* 5812-5817, 2010.
14. Russell, R., Johnson, K., Durbin, T., Chen, P. et al., "Emissions, Fuel Economy, and Performance of a Class 8 Conventional and Hybrid Truck," SAE Technical Paper 2015-01-1083, 2015, doi:10.4271/2015-01-1083.
15. Zhang, X., Peng, H., Sun, J., and Li, S., "Automated Modeling and Mode Screening for Exhaustive Search of Double-Planetary-Gear Power Split Hybrid Powertrains," in *ASME 2014 Dynamic Systems and Control Conference*, 2014.
16. Honda, T., "Development of Handling Performance Control for SPORT HYBRID SH-AWD," SAE Technical Paper 2015-01-1575, 2015, doi:10.4271/2015-01-1575.
17. Halvorson, B., "2016 Lexus RX Hybrid F Sport First Drive,"2015, Available: http://www.greencarreports.com/news/1099941_2016-lexus-rx-hybrid-fsport-first-drive. [Online.Accessed 2016].
18. Alternative Fuels Data Center,"U.S. HEV Sales by Model,"2016[Online]. Available: http://www.afdc.energy.gov/data/.
19. Zhang, X., Li, C.-T., Kum, D., and Peng, H., "Prius+ and Volt-: Configuration Analysis of Power-Split Hybrid Vehicles with a Single Planetary Gear," *IEEE Transactions on Vehicular Technology* 61(8):3544-3552, 2012.
20. Zhang, X., Li, S.E., Peng, H., and Sun, J., "Efficient Exhaustive Search of Power-Split Hybrid Powertrains with Multiple Planetary Gears and Clutches," *Journal of Dynamic Systems, Measurement, and Control* 137(12):121006, 2015.
21. Liu, J. and Peng, H., "A Systematic Design Approach for Two Planetary Gear Split Hybrid Vehicles," *Vehicle System Dynamics* 48(11):1395-1412, 2010.
22. Jalil, N., Kheir, N.A., and Salman, M., "A Rule-Based Energy Management Strategy for a Series Hybrid Vehicle," in *American Control Conference*, 1997, 689-693.
23. Sciarretta, A., Back, M., and Guzzella, L., "Optimal Control of Parallel Hybrid Electric Vehicles," *IEEE Transactions on Control Systems Technology* 12(3):352-363, 2004.
24. Stockar, S., Marano, V., Rizzoni, G., and Guzzella, L., "Optimal Control for Plug-in Hybrid Electric Vehicle Applications," in *American Control Conference (ACC)*, 2010, 5024-5030.
25. Lin, C.-C., Peng, H., Grizzle, J.W., and Kang, J.-M., "Power Management Strategy for a Parallel Hybrid Electric Truck," *IEEE Transactions on Control Systems Technology* 11(6):839-849, 2003.
26. Liu, J and Peng, H., "Control Optimization for a Power-Split Hybrid Vehicle," in *American Control Conference*, 2006, 6.
27. Bai, S., Maguire, J., and Peng, H., *Dynamic Analysis and Control System Design of Automatic Transmissions* (Warrendale: SAE International, 2013).
28. Yoshimura, T., "Vehicle Power Transmission," US20110314960A1, 2008.

Appendix

A. Calculation of Possible Power-Split Design Numbers

Given a double PG set, there are six nodes (ring gear node, carrier node, and sun gear node on each PG set) to be used to collocate four components (engine, two e-machines, and two output shafts, with an assumption that one e-machine is connected to one output shaft). Then, the total combinations are P_6^4. From those six nodes of the PG set, a placement of a clutch connects two out of the six nodes. Then, the total combination of a clutch connection is $C_6^5 = 15$. Furthermore, this manuscript presents the case using 3 clutch connections of the possible 15 connections. Therefore, the combination of three clutch connections is C_{15}^3. Because of the identical 2 PGs, all designs are repeated once. Therefore, the total number of designs is $0.5 \cdot P_6^4 \cdot C_{15}^3 = 81900$.

B. Calculation of the Average Acceleration

The 0-60 mph launching is divided into n speed grid evenly, as shown in Figure A.1.

For each speed grid, the velocity difference Δv of the initial value and the final value is known. In the ith speed grid, the time for this speed grid t_i can be calculated by Equation A.1,

$$t_i = \frac{v_i - v_{i-1}}{a_i} = \frac{\Delta v}{a_i} \qquad \text{Eq. (A.1)}$$

where a_i is the acceleration in this grid. The total time used for 0-60 mph launching is calculated in Equation A.2.

$$t_{tot} = \sum_{i=1}^{n} t_i = \Delta v \sum_{i=1}^{n} \frac{1}{a_i} \qquad \text{Eq. (A.2)}$$

By defining the average acceleration of the launching period shown in Equation A.3. The average acceleration relates a_i by Equation A.4.

FIGURE A.1 Speed grid division for evaluation of the average acceleration.

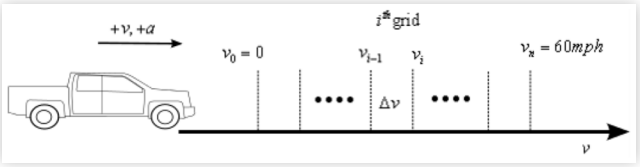

$$\bar{a} = \frac{v_n - v_0}{t_{tot}} = \frac{n \cdot \Delta v}{t_{tot}} \qquad \text{Eq. (A.3)}$$

$$\bar{a} = \frac{n \cdot \Delta v}{t_{tot}} = \frac{n \cdot \Delta v}{\Delta v \sum_{i=1}^{n} \frac{1}{a_i}}$$

$$\Rightarrow \bar{a} = \frac{n}{\sum_{i=1}^{n} \frac{1}{a_i}} \qquad \text{Eq. (A.4)}$$

C. Model of Vehicle Dynamics for the Gradeability Tests

The gradeability tests in Figure A.2 are for a fully loaded vehicle driving on a slope with angle of θ. A free-body diagram for the tow-vehicle motion is shown in Figure A.3.

The tow-vehicle has a trailer with weight of $m_T \cdot K_{cz}$ is the vertical internal force between the vehicle and the trailer body, and K_{cx} is that internal force in the longitudinal direction. Other symbols are defined in the same way as those in Section III. The subscript T refers to the front and rear tire reaction forces/torques, respectively. The gravitational constant is g, the aerodynamic force is D_A, T is the axle output torque, K_z is the vertical internal force between the wheels and body, K_x is the longitudinal internal force between the wheels and body, N_z is the tire reaction force in the vertical direction, and F_x is the tire reaction force in the longitudinal direction. The subscripts F and R refer to the front and rear tire reaction forces/torques, respectively.

Longitudinal dynamics and rotational motion dynamics of the vehicle body, the trailer, trailer wheels, front wheels, and rear wheels are given in Equations A.5 through A.19.

$$K_{x_f} + K_{x_r} - D_A - m_b g \sin\theta - K_{c_x} = m_b a \qquad \text{Eq. (A.5)}$$

FIGURE A.2 Gradeability tests of a full-loaded AWD tow vehicle.

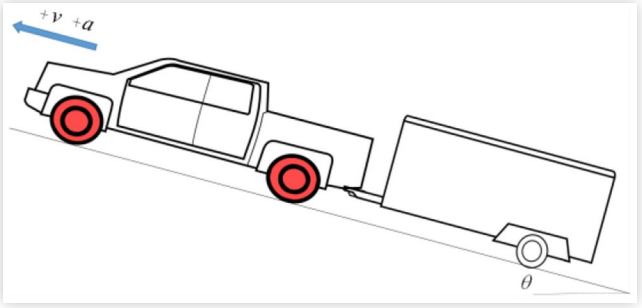

FIGURE A.3 Free-body diagram for the tow-vehicle motion on a slope.

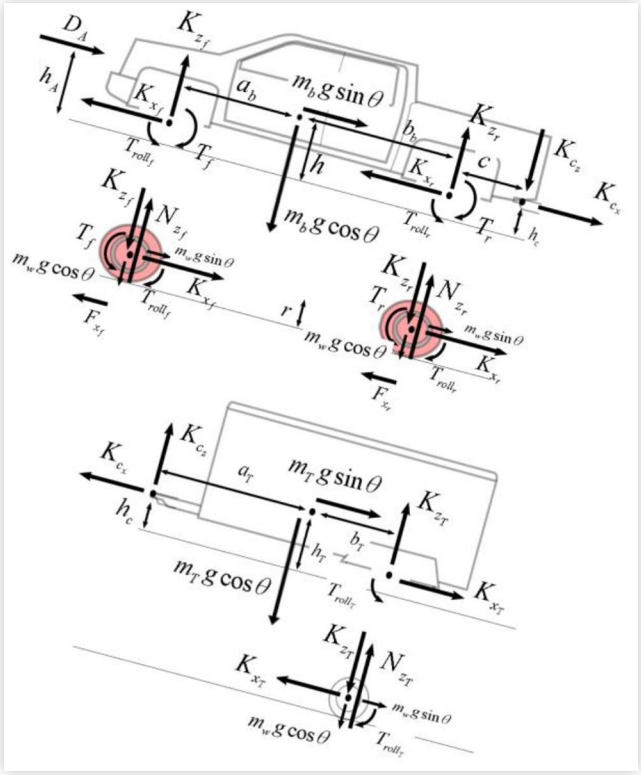

$$K_{z_f} + K_{z_r} - K_{c_z} = m_b g\cos\theta \qquad \text{Eq. (A.6)}$$

$$-K_{z_f} a_b + K_{z_r} b_b - D_A\left(h_A - h\right) - \left(K_{x_f} + K_{x_r}\right)\cdot\left(h - r\right) + T_f - T_{roll_f} + T_r - T_{roll_r} - K_{c_z}\left(b + c\right) + K_{c_x}\left(h_A - h_T\right) = 0 \qquad \text{Eq. (A.7)}$$

$$T_f - F_{x_f} r - T_{roll_f} = I_w \dot{\omega}_f \qquad \text{Eq. (A.8)}$$

$$F_{x_f} - K_{x_f} = m_w a \qquad \text{Eq. (A.9)}$$

$$N_{z_f} - K_{z_f} - m_w g\cos\theta = 0 \qquad \text{Eq. (A.10)}$$

$$T_r - F_{x_r} r - T_{roll_r} = I\dot{\omega}_r \qquad \text{Eq. (A.11)}$$

$$F_{x_r} - K_{x_r} = m_w a \qquad \text{Eq. (A.12)}$$

$$N_{z_r} - K_{z_r} - m_w g\cos\theta = 0 \qquad \text{Eq. (A.13)}$$

$$K_{c_x} - m_T g\sin\theta - K_{x_T} = m_T a \qquad \text{Eq. (A.14)}$$

$$K_{c_z} + K_{z_T} = m_T g\cos\theta \qquad \text{Eq. (A.15)}$$

$$K_{z_T} b_T - K_{x_T}\cdot\left(h_T - r\right) - T_{roll_T} - K_{c_z} a_T + K_{c_x}\left(h_T - h_c\right) = 0 \qquad \text{Eq. (A.16)}$$

$$F_{x_T} r - T_{roll_T} = I_w \dot{\omega}_T \qquad \text{Eq. (A.17)}$$

$$K_{x_T} - F_{x_T} = m_w a \qquad \text{Eq. (A.18)}$$

$$N_{z_T} - K_{z_T} - m_w g\cos\theta = 0 \qquad \text{Eq. (A.19)}$$

The maximum driving forces for the three cases (i.e., AWD, FWD, and RWD) in the gradeability tests are shown in Table A.1.

TABLE A.1 Maximum driving forces.

Hybrid vehicle drivetrain designs	Max tire forces
AWD	$F_{AWD\_max} = N_{zf} \cdot \mu_{tire} + N_{zr} \cdot \mu_{tire}$
FWD	$F_{FWD\_max} = N_{zf} \cdot \mu_{tire}$
RWD	$F_{RWD\_max} = N_{zr} \cdot \mu_{tire}$